Feeding of Rh and Ag isomers in fast-neutron-induced reactions

N. Fotiades, M. Devlin, R. O. Nelson, T. Kawano, and J. J. Carroll

Phys. Rev. C **94**, 044608 — Published 17 October 2016

DOI: 10.1103/PhysRevC.94.044608

Feeding of Rh and Ag isomers in fast neutron-induced reactions.

N. Fotiades,* M. Devlin, R. O. Nelson, and T. Kawano

Los Alamos National Laboratory, Los Alamos, New Mexico 87545, USA

J. J. Carroll

US Army Research Laboratory, Adelphi, MD 20783, USA

Abstract

Background: In (n, n') reactions on stable Ir and Au isotopes in the mass $A = 190$ region the experimentally established feeding of the isomers relative to the feeding of the corresponding ground states increases with increasing neutron energy up to the neutron energy where the $(n, 2n)$ reaction channel opens up and then decreases.

Purpose: In order to check for similar behavior in the mass $A = 100$ region the feeding of isomers and ground states in fast-neutron-induced reactions on stable isotopes in this mass region was studied. This is of especial interest for Rh which can be used as a radiochemical detector.

Methods: Excited states were studied using the $(n, n'\gamma)$, $(n, 2n\gamma)$ and $(n, 3n\gamma)$ reactions on ^{103}Rh and ^{109}Ag. A germanium-detector array for γ-ray detection and the broad-spectrum pulsed neutron source of the Los Alamos Neutron Science Center's Weapons Neutron Research facility were used for the measurement. The energy of the incident neutrons was determined using the time-of-flight technique.

Results: Absolute partial γ-ray cross sections were measured for 57 transitions feeding isomers and ground states in ^{101,102,103}Rh and ^{107,108,109}Ag. The feeding of the isomers was found to be very similar in the corresponding reaction channels and it is compared to the feeding determined for the ground states.

Conclusions: The opening of reaction channels at higher neutron energies removes angular momentum from the residual nucleus and reduces the population of the higher-spin isomers relative to the feeding of the lower-spin ground states. Similar behavior was observed in the mass $A = 190$ region in the feeding of higher-spin isomers, but the reverse behavior was observed in ^{176}Lu with a lower-spin isomer and a higher-spin ground state.

PACS numbers: PACS number(s): 25.40.-h, 28.20.-v, 24.10.-i, 25.40.Fq

*fotia@lanl.gov

I. INTRODUCTION

The study of fast neutron-induced reactions, especially at higher incident energies, is of interest to both basic and applied nuclear physics. In basic nuclear physics neutron-induced reactions can be used to characterize reaction mechanisms and investigate nuclear structure by imposing constraints on nuclear models. Because of the difficulty in predicting nuclear structure effects that can influence the population of various states it is important to have data to constrain reaction models that predict nuclear level populations. For instance, in (n, n') reactions in the mass $A = 190$ region similarities were observed in the feeding of the $11/2^-$ isomers of ^{191}Ir, ^{193}Ir and ^{197}Au that suggest similar level densities in the continua that feed the isomers and similar underlying low-excitation-energy nuclear structure [1]. The feeding of these isomers relative to the feeding of the corresponding ground states increases with increasing neutron energy up to the opening of the $(n, 2n)$ reaction channel and decreases above it. Hence, the opening of the $(n, 2n)$ channel diminishes the population of the higher-spin $11/2^-$ isomers relative to the population of the lower-spin ground states in ^{191}Ir, ^{193}Ir and ^{197}Au. In order to check for similar behavior in other mass regions the feeding of isomers and ground states in similar reactions needs to be determined. For applications, cross sections of (n, xn) reactions are necessary, e.g. for activation detectors (also known as radiochemical detectors) which are used to probe energy components of a neutron fluence. An example of such a detector is rhodium, which is monoisotopic.

^{103}Rh [2] has been used as a radiochemical diagnostic of integrated neutron fluence because the capture reaction (n, γ) and the $(n, 2n)$ and $(n, 3n)$ reactions all lead to isotopes of rhodium with lifetimes in the useful range for neutron activation measurements. In ^{102}Rh [3] there is a 140.73 keV, $6^{(+)}$ level with a lifetime of 3.742 y. The ground state has spin and parity (1^-,2^-) and a lifetime of 207.3 d. The relatively large difference in the spins means that $(n, 2n)$ reactions on the isomer and ground state populate rather different sets of levels in the final nucleus and will likely have different reaction cross sections. The resulting activation probability for a rapidly time-varying neutron fluence is then a neutron-energy-dependent, weighted (by the relative populations) sum of the $(n, 2n)$ cross sections of the ground and isomeric states. No other long-lived isomers are known in ^{102}Rh. Previous measurements of the population of the 140.73 keV isomeric state have been reported, the most extensive neutron-energy-range set is in Ref. [4]. The measured cross-section values vary between

$\sim$0.4 b [4] and $\sim$0.7 b [5] at $\sim$14 MeV neutron energy. In the $(n, 3n)$ reaction producing ^{101}Rh [6], the first excited state is at 157.32 keV excitation energy, a $9/2^+$, 4.34 d isomer. The ^{101}Rh ground state has spin and parity $1/2^-$ with a lifetime of 3.3 y. Here, again, a large spin difference is the case, while no other long-lived isomers are known. As for ^{102}Rh, the $(n, 3n)$ neutron activation probability includes feeding of the isomeric state. No data exist for the population of this isomeric state via neutron-induced reactions. For the stable ^{103}Rh [2], the first excited state is at 39.75 keV excitation energy, a $7/2^+$, 56.114 min isomer and the ground state has spin and parity $1/2^-$.

The nuclear structure in neighboring stable Ag isotopes is similar at low excitation energies leading to observation of isomers of similar spins but of different half-lives. In ^{108}Ag [7] the second excited state is a 109.47 keV, 6^+ level with a lifetime of 438 y. This long half-life makes ^{108}Ag important when considering storage of radioactive waste from nuclear power plants [8]. The ground state of ^{108}Ag has spin and parity 1^+ and a lifetime of 2.38 min. The shorter lifetime here, compared to the one in ^{102}Rh, renders this isotope not as useful for radiochemical detection, but perhaps of interest for induced energy release [9]. In the stable isotopes ^{107}Ag [10] and ^{109}Ag [11] the first excited states are at 93.12- and 88.03-keV excitation energy, respectively, and are $7/2^+$ isomers with 44.3- and 39.6-s half-lives, respectively. The ground states have spin and parity $1/2^-$ in both isotopes.

Partial γ-ray cross sections for low-lying states (in particular 2^+ to 0^+ ground-state transitions in even-even nuclei) often can be used to accurately infer reaction channel cross sections because a very large fraction of all γ-ray decays pass through the 2^+ first-excited state (see, for instance, Ref. [12], and references therein). For more complicated cases, in which the decay scheme involves many more levels, nuclear reaction model calculations were tested and combined with the measured γ-ray data to infer more accurate (n, xn) cross sections (see, for instance, Ref. [13]). The Rh and Ag isotopes are such complicated cases because they are all odd-mass or odd-Z-odd-N nuclei. The present data provide useful lower limits on the population of the isomeric and ground states, and combined with model calculations, can give an estimate of the total population.

II. EXPERIMENTS

The γ rays produced in the bombardment of the ^{103}Rh and ^{109}Ag targets by neutrons were measured with the GEANIE spectrometer [14]. GEANIE was located 20.34 m from the Los Alamos Neutron Science Center's Weapons Neutron Research (LANSCE-WNR) facility's spallation neutron source [15, 16] on the 60R (60°-Right) flight path. The neutrons were produced in a ^{nat}W spallation target driven by an 800 MeV proton beam. The beam time structure consisted of 625 μs-long "macropulses" at 40 Hz rate. Each macropulse contained approximately 340 "micropulses" spaced every 1.8 μs. At this "micropulse" spacing, wrap-around problems (time overlap of high-energy neutrons of one pulse with lower-energy neutrons of the previous pulse) start at $E_n \sim 0.6$ MeV and below. The energy of the neutrons was determined using the time-of-flight (TOF) technique. A schematic diagram of the experimental setup can be found in Ref. [17]. GEANIE was comprised of 10 Compton suppressed planar Ge detectors (low-energy photon spectrometers, or LEPS) and 10 Compton suppressed coaxial Ge detectors. During the ^{103}Rh experiment 6 unsuppressed coaxial Ge detectors were also used, however, four of the total 26 detectors were not used in the analysis of the data for reasons of "poor" resolution or frequent gain shifting during the experiment. For the same reasons, nine of the total 20 detectors were not used in the analysis of the data in the ^{109}Ag experiment.

In the ^{103}Rh experiment the target consisted of two 2.5 cm square foils of 1.58 g of ^{103}Rh. During two days of the experiment, two natural Fe 2.5 cm square foils, 0.05 mm thick each, were placed, in front and in back of the ^{103}Rh foils. The Fe foils were included so that the known cross section at $E_n = 14.5$ MeV (see Ref. [18], and references therein) of the strong 846.8-keV, $2^+ \rightarrow 0^+$ transition of ^{56}Fe, produced in natural Fe from inelastic scattering, could be used to normalize the cross sections obtained in the present experiment. In the ^{109}Ag experiment the target consisted of one 2.22 cm square foil of 1.35 g of ^{109}Ag enriched to 99.26%. The same Fe foils were placed in front and in back of the ^{109}Ag foil during two days of the experiment. All targets were at an angle of 90^o with respect to the beam. The Rh, Ag and Fe foils were larger than the beam spot.

The neutron flux on targets was measured with a fission chamber, consisting of ^{235}U and ^{238}U foils [19], located 18.5 m from the center of the spallation target. Detector efficiencies were determined using a variety of calibrated γ-ray reference sources. Data acquisition

system "dead-times" were measured using scalers. During the experiments the data were stored for subsequent off-line analysis. A total of $\sim 5.5 \times 10^8$ and $\sim 7 \times 10^8$ γ singles and higher fold data were recorded in the ^{103}Rh, and ^{109}Ag experiments, respectively. The off-line analysis described in Ref. [17] was applied to all data-sets.

III. EXPERIMENTAL RESULTS

The cross sections for emission of a total of 33 γ rays of ^{101,102,103}Rh and 24 γ rays of ^{107,108,109}Ag were determined. The observed γ rays are included in the level schemes in Figs. 1 and 2. Twenty transitions from Figs. 1 and 2 can be identified in the γ-ray spectra in Fig. 3 which are summed over all neutron energies. Examples of the partial cross sections obtained for some of the transitions in Figs. 1 and 2 are shown in Figs. 4 and 5. The sum of the cross sections obtained for the transitions that feed the isomers and ground states in Figs. 1 and 2 are shown in Figs. 6, 7, and 8. The uncertainties in the cross section values presented in Figs. 6, 7, and 8 are statistical from the γ-ray yields. Systematic uncertainties originate from γ-ray absorption in the samples, γ-ray internal conversion corrections, finite beam size effects, detector efficiencies, neutron fluences (include uncertainties in the fission foil thickness, fission cross section, and ionization chamber efficiency), target thicknesses and "dead-times", that can be different for the two experiments and were estimated to be less than a total of 15% in all cases.

The 647.3- and 647.7-keV transitions form a doublet in the spectrum in Fig. 3.a, but since they belong to the (n, n') and $(n, 3n)$ reaction channels, respectively (see Fig. 2.a and c), their feeding contributions can be separated by gating at different neutron energies. However, some transitions form unresolved doublets even in neutron-energy-gated γ-ray spectra, e.g., the two 590.4-keV transitions of ^{101}Rh (see Fig. 1.c). Both transitions feed the ^{101}Rh isomer directly and, hence, the deduced partial cross section for the 590.4-keV doublet observed in the γ-ray spectra can be included in the sum of cross sections to determine the feeding of the isomer. Another example of unresolved doublets are the 156.5- and 156.6-keV transitions of ^{102}Rh in Fig. 1.b which feed ground state and isomer, respectively. The cross section of the former can be estimated from the experimentally obtained cross section for the 51.27-keV transition emitted from the same level of ^{102}Rh and using the known relative intensities of the two transitions [3]. Thus, the cross section for the 156.6-keV transition can

then be deduced by subtraction from the total cross section obtained for the double peak in the spectra. Finally, the contribution in the feeding of some low-energy transitions that were not observed in the spectra due to internal conversion was approximated by the inclusion of transitions that feed the corresponding emitting levels. For instance, the 13.7-keV transition that is emitted from the 154-keV level of ^{102}Rh [3] to the isomer in Fig. 1.b was not observed and its contribution was estimated from the 205.1-, 223.6-, and 528.4-keV transitions, and also, the 32.46-keV transition emitted from the 126-keV level of ^{107}Ag [10] in Fig. 2.c whose contribution was estimated from the 647.7- and 865.4-keV transitions.

IV. DISCUSSION

The sum of the prompt γ-ray cross sections obtained for the transitions in the (n, n') and $(n, 3n)$ channels in both experiments is expected to represent a considerable portion of the total cross section that populates the corresponding isomers and ground states. These sums represent a percentage of the total population of the channels and need to be corrected for the strength of weak or unknown transitions that are not observed in order to deduce the total population. In Figs. 6, 7, and 8 the experimentally observed sums are compared with estimates for the total channel population taken from evaluated libraries [20, 21]. In the $(n, 2n)$ channels in both experiments, the populated ^{102}Rh and ^{108}Ag isotopes are odd-odd nuclei and are expected to exhibit higher level fragmentation in their level schemes with more weak transitions that feed the isomers and ground states being below the detection limit in both experiments. Hence, the experimentally obtained sums of prompt γ-ray cross sections represent a lower percentage of the total population of the $(n, 2n)$ channels, as shown in Fig. 7.

The sum of the cross sections that feed the isomers were divided by the sum of the cross sections that feed the ground states of ^{101,102,103}Rh and ^{107,108,109}Ag at each neutron energy. The resulting ratios are shown in Figs. 9, 10 and 11 and exhibit striking similarities in both experiments. Specifically, at low neutron energies the isomers, being higher-spin states compared to the ground states, are populated weakly in all reaction channels. However, as the incident neutron energy and, hence, the angular momentum increase, the population of the isomers increases relative to the population of the ground states. This increase in isomer population continues up to the incident-neutron energy where other reaction channels open

up. For instance, for the ^{103}Rh experiment, there are 15 reaction channels with a threshold less than 10 MeV, at 20 MeV neutron energy there are 55 reaction channels open, and at 40 MeV 290 channels. In Figs. 9, 10 and 11 at higher neutron energies the relative population of the isomers decreases suggesting that the opening of additional reaction channels affects more the population of the isomers. Hence, the opening of the reaction channels at higher neutron energies appear to remove angular momentum from the residual nucleus and reduce the population of the isomers because they are higher-spin states.

A calculation at various neutron energies of all the possible reaction paths using the code CoH_3 [22] predicts the production cross sections for each channel in Fig. 12. It is not straightforward from this calculation to determine which reaction channel or channels are responsible for the observed behavior, although a big part of the (n, n')-, $(n, 2n)$- and $(n, 3n)$-channel cross section is carried away mainly by the opening of the $(n, 2n)$, $(n, 3n)$, and $(n, 4n)$ channels, respectively, as can be seen in Fig. 12 for both the ^{103}Rh and ^{109}Ag reaction channels. It is also noteworthy that in Fig. 12 the cross section for the $(n, 3n)$ channels becomes comparable to that for the $(n, 2n)$ channels at $E_n \sim 21$ MeV. In Fig. 10 the feeding of the isomers peaks at about the same neutron-induced energy. Similarly, in Fig. 12 the cross section for the $(n, 4n)$ channels becomes comparable to that for the $(n, 3n)$ channels at $E_n \sim 34$ MeV and in Fig. 11 the feeding of the isomers peaks at about the same neutron-induced energy.

Similar calculations to those in Fig. 12 but for the ^{191,193}Ir [23, 24] and ^{197}Au [25] isotopes indicate that the cross sections for the $(n, 4n)$ channels become comparable to those in the $(n, 3n)$ channels at $E_n \sim 28$ MeV, as it is shown for the case of ^{197}Au in Fig. 13. In all calculations described in the present work the global deformed optical potential from Ref. [26] was adopted to calculate the neutron transmission coefficients. The coupled-channels calculation was performed with the deformation parameters taken from the finite range droplet model [27]. For charged particle emission channels the Koning-Delaroche potential [28] for proton, the Becchetti-Greenlees potential [29] for ^{3}He and triton, the α-particle potential from Ref. [30] and the deuteron potential from Ref. [31] were used. For the heavier targets (Au and Ir) the composite particle emission channels were ignored due to the large Coulomb barrier. The level densities were calculated with the composite level density formulae of Gilbert and Cameron [32] with an updated parametrization [33]. The level density parameters were further tuned to reproduce the evaluated average s-wave resonance spacing

D_0 [34]. At low excitation energies the discrete level data were taken from the evaluated nuclear structure database RIPL-3 [35]. The γ-ray transmission coefficients were calculated from the γ-ray strength functions. For the double-humped $E1$ strength a generalized Lorentzian form [36] was adopted. The giant dipole resonance parameters were taken from the RIPL-3 library [35]. The higher multipolarities $M1$, $E2$, $M2$, and $E3$ in the standard Lorentzian shape were included. For the pre-equilibrium process the two-component exciton model [37] was used with the single-particle state density parameters determined by the Strutinsky method [38].

In Ref. [1], the feeding of the isomers in the $(n, 3n)$ channels was not studied, however, an extended analysis of the data from Ref. [1] in the present work revealed that the feeding of the isomers in the $(n, 3n)$ channels peaks at about the same neutron-induced energy, as can be seen in Fig. 13 for ^{195}Au [39] and ^{189}Ir [40]. Hence, in all cases studied here and in both mass regions the feeding of the isomers in the $(n, 3n)$ channels is affected mostly by the opening of the corresponding $(n, 4n)$ channels and the effect becomes detectable by the peaking of the feeding ratios in Figs. 11 and 13 around the neutron-induced energy where the cross sections for the $(n, 3n)$ and corresponding $(n, 4n)$ channels are predicted by the calculations to become comparable. Because of the presence of more than one isomer in ^{196}Au [41] and ^{190,192}Ir [42, 43] at low excitation energies the feeding ratios for the corresponding isomers in the $(n, 2n)$ channels in the GEANIE experiments described in Ref. [1] were impossible to deduce during the extended analysis attempted here. Hence, similar conclusions for the $(n, 2n)$ channels can be drawn from the present work but are limited only to the mass $A = 100$ region.

The similarities in the feeding of the transitions that feed the isomers in all isotopes in Figs. 1 and 2 could arise from similarities in the level densities and the spin and parity distributions in the continuum of states that feed these states. Similar underlying nuclear structure is also necessary toward this end. This is especially true for high-spin states whose population can only come from a few high-spin states higher in energy. Such an observation requires extensive nuclear modeling work in order to be quantified and lies beyond the scope of the present work. Assuming that the level densities and the spin and parity distribution in the continuum of states do not change drastically in neighboring odd-mass isotopes a similar behavior in the feeding of low-lying higher-spin isomers in these isotopes can be expected. On the other hand, in isotopes with low-lying isomers with spins lower than the spin of the

corresponding ground states (e.g., in ^{176}Lu [44]), the reverse behavior could exist, namely the feeding of the isomer relative to the feeding of the corresponding ground state decreases with increasing neutron energy up to the neutron energy where the $(n, 2n)$ reaction channel opens up and then increases. Indeed, as was reported in a conference recently [45] the behavior shown in Fig. 14 was observed in a ^{nat}Lu GEANIE experiment. However, ^{nat}Lu contains only 2.59% of ^{176}Lu and the rest is ^{175}Lu, hence, only three transitions of ^{176}Lu were observed, namely the 184.1-keV transition that feeds directly the 7^- ground state, and the 112.9- and 310.2-keV transitions that feed directly the 1^- isomer. Hence, the statistics in the feeding ratio in Fig. 14 are not as good as those in the other cases studied here. Nevertheless, the reverse behavior compared to the rest of the cases studied in the present work, can be clearly observed in Fig. 14.

V. SUMMARY

In conclusion, partial γ-ray cross sections were measured for several transitions feeding in parallel isomers and ground states of ^{101,102,103}Rh and ^{107,108,109}Ag in fast-neutron-induced reactions on ^{103}Rh and ^{109}Ag. A comparison of the population of the isomers was made. In the (n, n') channels the feeding of the isomers relative to the feeding of the corresponding ground states increases with increasing neutron energy up to $E_n \sim 9$ MeV. Above this neutron energy the opening of the $(n, 2n)$ reaction channel affects more the population of the isomers and leads to a decrease of their relative population. Similar behavior has been observed in the mass $A = 190$ region. The feeding of the isomers was found to be very similar in all corresponding reaction channels when compared to the feeding determined for the ground states. The opening of the $(n, 4n)$ reaction channel appears to be the main reason for the observed diminishing of the feeding of the isomers in the $(n, 3n)$ reaction channels in all cases studied. Generally, the opening of reaction channels at higher neutron energies removes angular momentum from the residual nucleus and reduces the population of the higher-spin isomers relative to the feeding of the lower-spin ground states in all cases. The reverse scenario could unfold in isotopes with low-lying isomers of lower spin than the spin of the corresponding ground states.

Acknowledgments

This work was performed under the auspices of the U.S. Department of Energy (DOE) under Contract No. DE-AC52-06NA25396. This work has benefitted from use of the LANSCE accelerator facility supported under DOE Contract No. DE-AC52-06NA25396. The enriched ^{109}Ag target was provided by Ecopulse, Inc. under US Army Research Laboratory Contract No. W911QX09D0016-0003.

---

[1] N. Fotiades, R. O. Nelson, M. Devlin, S. Holloway, T. Kawano, P. Talou, M. B. Chadwick, J. A. Becker, and P. E. Garrett, Phys. Rev. C **80**, 044612 (2009).

[2] D. De Frenne, Nucl. Data Sheets 110, 2081 (2009).

[3] D. De Frenne, Nucl. Data Sheets 110, 1745 (2009).

[4] A. Paulsen and R. Widera, Z. Phys. **238**, 23 (1970).

[5] M. Bormann, H. H. Bissem, E. Magiera, and R. Warnemünde, Nucl. Phys. **A157**, 481 (1970).

[6] J. Blanchot, Nucl. Data Sheets 83, 1 (1998).

[7] J. Blanchot, Nucl. Data Sheets 91, 135 (2000).

[8] L. Ferreux, M.-C. Lépy, M.-M. Bé, H. Isnard, and V. Lourenço, Appl. Radiat. Isot., 87, 101 (2014).

[9] J. J. Carroll *et al.*, AIP Conf. Proc. **1525**, 586 (2013).

[10] J. Blanchot, Nucl. Data Sheets 109, 1383 (2008).

[11] J. Blanchot, Nucl. Data Sheets 107, 355 (2006).

[12] N. Fotiades, M. Devlin, R. C. Haight, R. O. Nelson, S. Kunieda, and T. Kawano, Phys. Rev. C **91** 064614 (2015).

[13] H. Vonach, A. Pavlik, M. B. Chadwick, R. C. Haight, R. O. Nelson, S. A. Wender, and P. G. Young, Phys. Rev. C **50**, 1952 (1994).

[14] J. A. Becker and R. O. Nelson, Nucl. Phys. News International **7**, 11 (1997).

[15] P. W. Lisowski, C. D. Bowman, G. J. Russell, and S. A. Wender, Nucl. Sci. Eng. **106**, 208 (1990).

[16] P. W. Lisowski and K. F. Schoenberg, Nucl. Instrum. Methods Phys. Res., Sect. A **562**, 910 (2006).

[17] N. Fotiades *et al.*, Phys. Rev. C **69**, 024601 (2004).

[18] R. O. Nelson, N. Fotiades, M. Devlin, J. A. Becker, P. E. Garrett, and W. Younes, AIP Conf. Proc. **769**, 838 (2005).

[19] S. A. Wender, S. Balestrini, A. Brown, R. C. Haight, C. M. Laymon, T. M. Lee, P. W. Lisowski, W. McCorkle, R. O. Nelson, and W. Parker, Nucl. Instrum. Methods Phys. Res. A **336**, 226 (1993).

[20] Special Issue on ENDF/B-VII.1 Library, edited by P. Obložinský, Nucl. Data Sheets 112, 2887-3152 (2011).

[21] The JEFF-3.1.1 Nuclear Data Library, edited by A. Santamarina, D. Bernard, and Y. Rugama, ISBN 978-92-64-99074-6 (2009).

[22] T. Kawano *et al.*, J. Nucl. Sci. Technol. (Abingdon, UK) **47**, 462 (2010).

[23] V. R. Vanin, N. L. Maidana, R. M. Castro, E. Achterberg, O. A. Capurro, and G. V. Marti, Nucl. Data Sheets **108**, 2393 (2007).

[24] E. Achterberg, O. A. Capurro, G. V. Marti, V. R. Vanin, and R. M. Castro, Nucl. Data Sheets **107**, 1 (2006).

[25] X. Huang and C. Zhou, Nucl. Data Sheets **104**, 283 (2005).

[26] S. Kunieda, S. Chiba, K. Shibata, A. Ichihara, and E. Sh. Sukhovitskii, J. Nucl. Sci. Technol. (Tokyo) **44**, 838 (2007).

[27] P. Möller, J. R. Nix, W. D. Myers, and W. J. Swiatecki, At. Data and Nucl. Data Tables **59**, 185 (1995).

[28] A. Koning and J.-P. Delaroche, Nucl. Phys. **A713**, 231 (2003).

[29] F. D. Becchetti and G. W. Greenlees, in *Polarization Phenomena in Nuclear Reactions*, edited by H. H. Barschall and W. Haeberli, The University of Wisconsin Press, Madison (1971).

[30] M. Avrigeanu, A. C. Obreja, F. L. Roman, V. Avrigeanu, and W. von Oertzen, At. Data Nucl. Data Tables **95**, 501 (2009).

[31] J. Bojowald, H. Machner, H. Nann, W. Oelert, M. Rogge, and P. Turek, Phys. Rev. C **38**, 1153 (1988).

[32] A. Gilbert and A. G. W. Cameron, Can. J. Phys., **43**, 1446 (1965)

[33] T. Kawano, S. Chiba, and H. Koura, J. Nucl. Sci. Technol. (Tokyo) **43**, 1 (2006).

[34] S. F. Mughabghab, in *Atlas of Neutron Resonances, Resonance Parameters and Thermal Cross Sections, Z=1-100*, Elsevier (2006).

[35] Reference Input Parameter Library (RIPL-3), International Atomic Energy Agency, Nuclear Data Services, https://www-nds.iaea.org/RIPL-3/

[36] J. Kopecky and M. Uhl, Phys. Rev. C, **41**, 1941 (1990).

[37] A. J. Koning and M.C. Duijvestijn, Nucl. Phys. A **744**, 15 (2004).

[38] T. Kawano, Eur. Phys. J. A **51**, 164 (2015).

[39] X. Huang and M. Kang, Nucl. Data Sheets **121**, 395 (2014).

[40] S.-C. Wu and H. Niu, Nucl. Data Sheets **100**, 1 (2003).

[41] X. Huang, Nucl. Data Sheets **108**, 1093 (2007).

[42] B. Singh, Nucl. Data Sheets **99**, 275 (2003).

[43] C. M. Baglin, Nucl. Data Sheets **113**, 1871 (2012).

[44] M. S. Basunia, Nucl. Data Sheets **107**, 791 (2006).

[45] N. Fotiades *et al.*, Bull. Am. Phys. Soc. **54**, No 10, 166 (2009).

FIG. 1: Partial level schemes showing the transitions of Rh isotopes relevant to the present work. All γ-ray and level energies are given in keV. The white portion of the arrows indicates the fraction of the decay that is internally converted. Data taken from Ref. [2] in a, from Ref. [3] in b, and from Ref. [6] in c.

FIG. 2: Partial level schemes showing the transitions of Ag isotopes relevant to the present work. All γ-ray and level energies are given in keV. The white portion of the arrows indicates the fraction of the decay that is internally converted. Data taken from Ref. [11] in a, from Ref. [7] in b, and from Ref. [10] in c.

FIG. 3: Examples of γ-ray spectra summed over all neutron energies from the a) Ag and b) Rh experiments. Some of the transitions from Figs. 1 and 2 are indicated. The energies of the transitions are in keV. Unmarked peaks are transitions that are not of interest for the present work, i.e., their contribution to the feeding of ground states or isomers of the (n, n'), $(n, 2n)$ and $(n, 3n)$ reaction channels is already accounted for by other γ rays, or they belong to other reaction channels.

FIG. 4: Examples of absolute partial cross sections as a function of incident neutron energy for nine Rh transitions from Fig. 1. Bars along the E_n-axis represent the width of the neutron-energy bins in the TOF technique.

FIG. 5: Examples of absolute partial cross sections as a function of incident neutron energy for nine Ag transitions from Fig. 2. Bars along the E_n-axis represent the width of the neutron-energy bins in the TOF technique.

FIG. 6: Sums of cross sections obtained for the transitions in the level schemes in Figs. 1 and 2 prompt-feeding the $1/2^-$ ground states (open squares) and $7/2^+$ isomers (open diamonds) of a) ^{109}Ag and b) ^{103}Rh. The experimentally observed total feeding (sum of the previous two sums; solid circles) is then compared to the evaluated reaction channel cross section (solid lines) from the ENDF/B-VII.1 library (see Ref. [20], and references therein) in both cases. Legends apply to both panels. Bars along the E_n-axis represent the width of the neutron-energy bins in the TOF technique.

FIG. 7: Sums of cross sections obtained for the transitions in the level schemes in Figs. 1 and 2 prompt-feeding the ground states (open squares) and years-long-lived isomers (open diamonds) of a) ^{108}Ag and b) ^{102}Rh. The experimentally observed total feeding (sum of the previous two sums; solid circles) is then compared to the evaluated $(n, 2n)$ channel cross sections (solid lines) from the ENDF/B-VII.1 library (see Ref. [20], and references therein) in both cases. Legends apply to both panels. Bars along the E_n-axis represent the width of the neutron-energy bins in the TOF technique.

FIG. 8: Sums of cross sections obtained for the transitions in the level schemes in Figs. 1 and 2 prompt-feeding the $1/2^-$ ground states (open squares) of a) ^{107}Ag and b) ^{101}Rh, and the isomeric $7/2^+$ and $9/2^+$ states (open diamonds) of ^{107}Ag and ^{101}Rh, respectively. The experimentally observed total feeding (sum of the previous two sums; solid circles) is then compared to the evaluated $(n, 3n)$ channel cross section (solid lines) from the ENDF/B-VII.1 library (see Ref. [20], and references therein) and from the JEFF-3.1.1 library (see Ref. [21], and references therein). Legends apply to both panels. Bars along the E_n-axis represent the width of the neutron-energy bins in the TOF technique.

FIG. 9: Ratios of sums of cross sections obtained for the transitions prompt-feeding the $7/2^+$ isomers over the sums obtained for the transitions observed to feed promptly the $1/2^-$ ground states of ^{103}Rh (open squares) in Fig. 1 and ^{109}Ag (open circles) in Fig. 2. Bars along the E_n-axis represent the width of the neutron-energy bins in the TOF technique.

FIG. 10: Ratios of sums of cross sections obtained for the transitions prompt-feeding the years-long-lived isomers over the sums obtained for the transitions observed to feed promptly the ground states of ^{102}Rh (open squares) in Fig. 1 and ^{108}Ag (open circles) in Fig. 2. Bars along the E_n-axis represent the width of the neutron-energy bins in the TOF technique.

FIG. 11: Ratios of sums of cross sections obtained for the transitions prompt-feeding the $7/2^+$ isomer of ^{107}Ag and the $9/2^+$ isomer of ^{101}Rh over the sums obtained for the transitions observed to feed promptly the $1/2^-$ ground states of ^{107}Ag (open circles) in Fig. 2 and ^{101}Rh (open squares) in Fig. 1, respectively. Bars along the E_n-axis represent the width of the neutron-energy bins in the TOF technique.

FIG. 12: Production cross sections for various reaction channels predicted using the code CoH_3 [22] in neutron induced reactions of ^{103}Rh and ^{109}Ag. Only channels with a maximum cross section larger than 1 mb are shown. The reaction channels are shown in the legend while the emitted particles are included in the plot. Solid lines represent neutron-only-emitting channels, dotted lines include one proton emitted, dashed lines include one deuteron emitted, and dashed-dotted lines include one α-particle (short dashes) or one triton (long dashes) emitted. The long-dashed lines at low neutron energies represent neutron capture.

FIG. 13: Upper plot: production cross sections for various reaction channels predicted using the code CoH_3 [22] in neutron induced reactions of ^{197}Au. The reaction channels are shown in the legend while the emitted particles are included in the plot. Solid lines represent only-neutron-emitting channels and dotted lines include one proton emitted. Lower plot: Ratios of sums of cross sections obtained in GEANIE experiments described in Ref. [1] for the transitions prompt-feeding the $11/2^-$ isomers of ^{195}Au [39] and ^{189}Ir [40] over the sums obtained for the transitions observed to feed promptly the $3/2^+$ ground states of ^{195}Au (open circles) and ^{189}Ir (open squares), respectively. Specifically, the 180.1-, 261.8-, 439.5-, and 549.4-keV transitions that feed in parallel the ground state of ^{195}Au; the 207.1-, 387.9-, 560.3-, 628.3-, 749.5-, and 961.9-keV transitions that feed directly the $11/2^-$ isomer of ^{195}Au; the 94.3-, 113.8-, 300.5-, and 317.7-keV transitions that feed directly the ground state of ^{189}Ir; and the 243.5-, 364.8-, 459.5-, and 466.0-keV transitions that feed directly the $11/2^-$ isomer of ^{189}Ir, were used. Bars along the E_n-axis represent the width of the neutron-energy bins in the TOF technique.

FIG. 14: Ratio of the sum of cross sections obtained for two transitions feeding directly the 1^- isomer over the cross section obtained for one transition observed to feed directly the 7^- ground state in ^{176}Lu. Specifically, the 112.9- and 310.2-keV transitions feed directly the 1^- isomer and the 184.1-keV transition feeds directly the 7^- ground state. Data from a ^{nat}Lu GEANIE experiment [45]. Bars along the E_n-axis represent the width of the neutron-energy bins in the TOF technique.

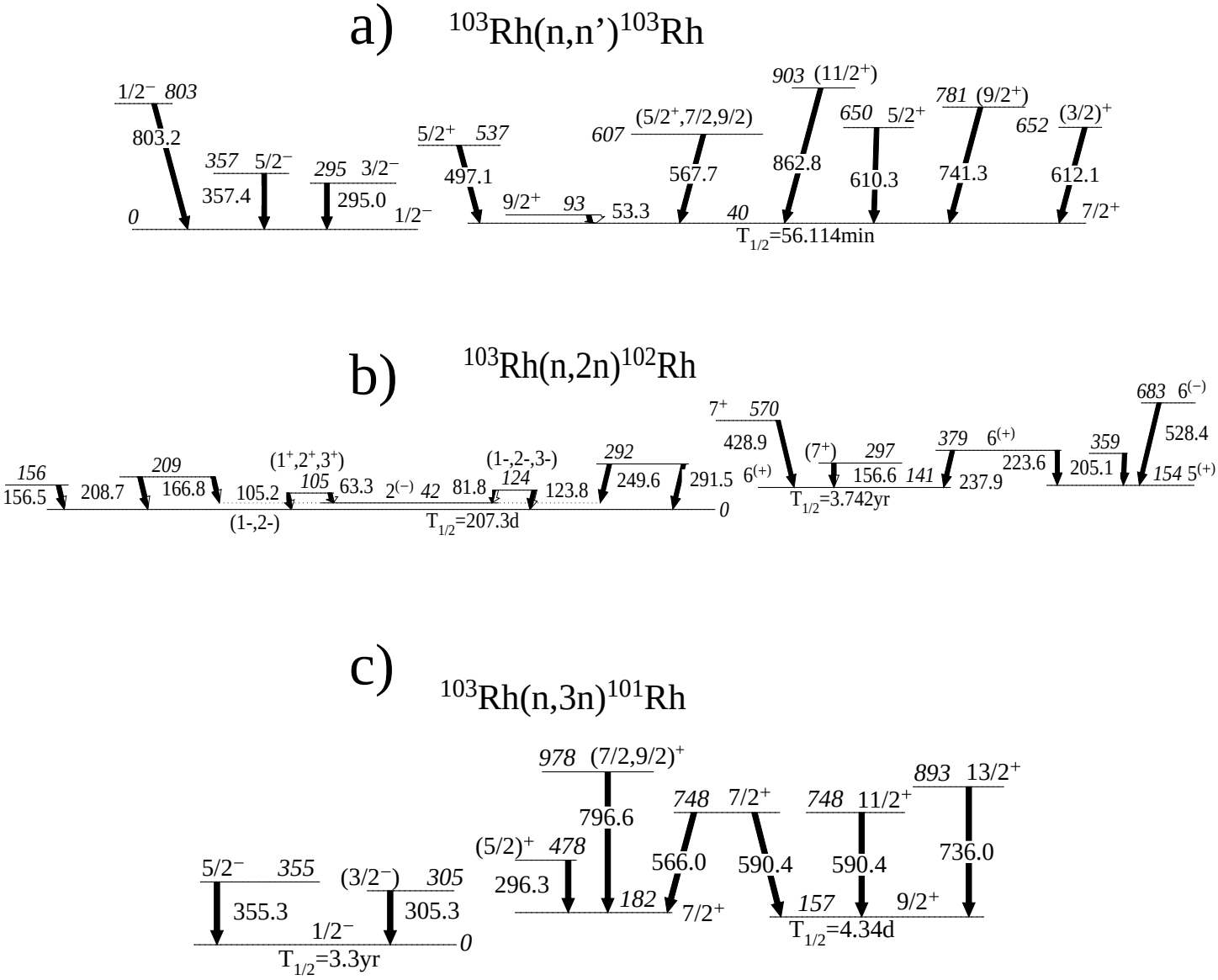

Figure 1 28Jul2016

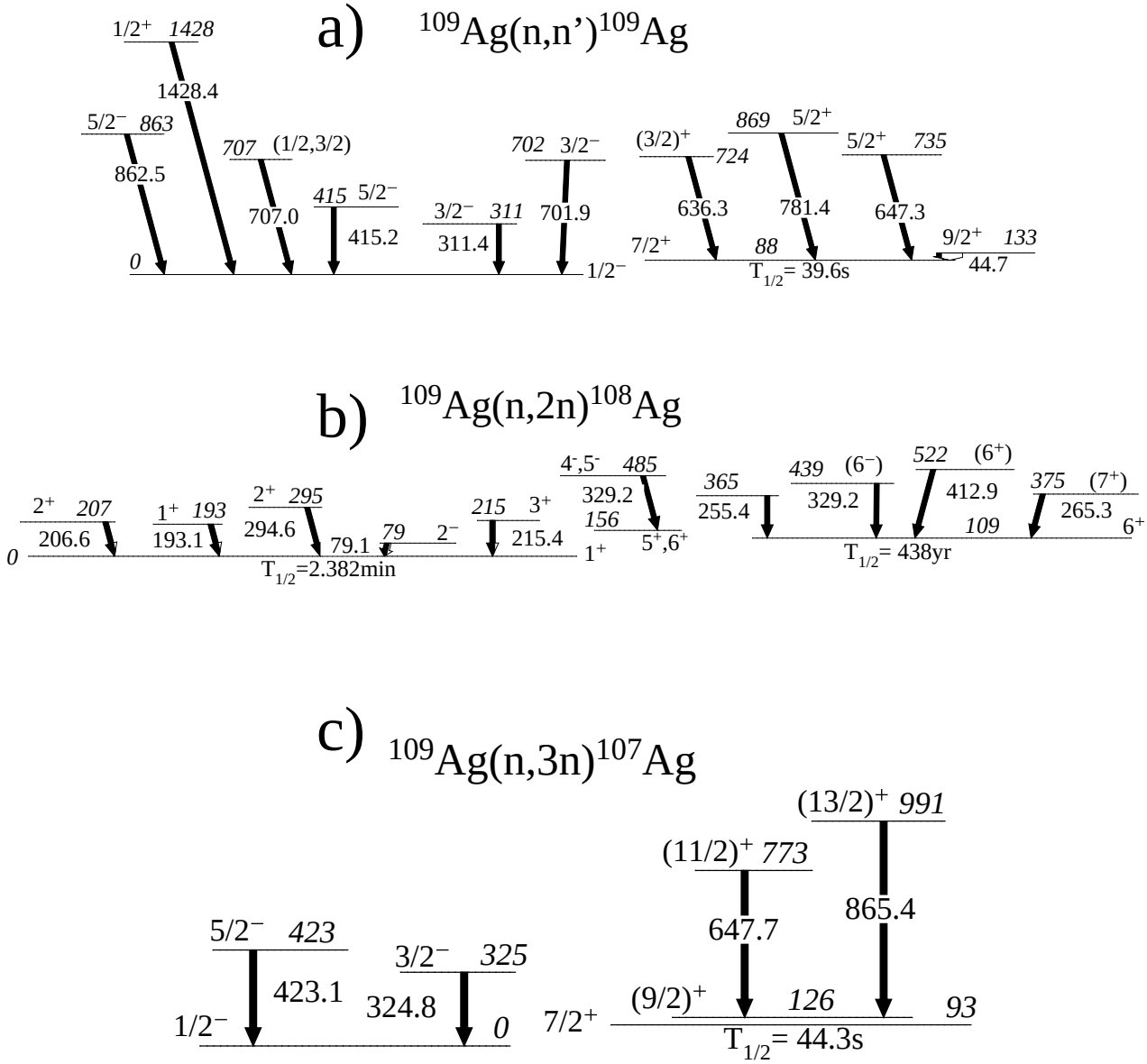

Figure 2 28Jul2016

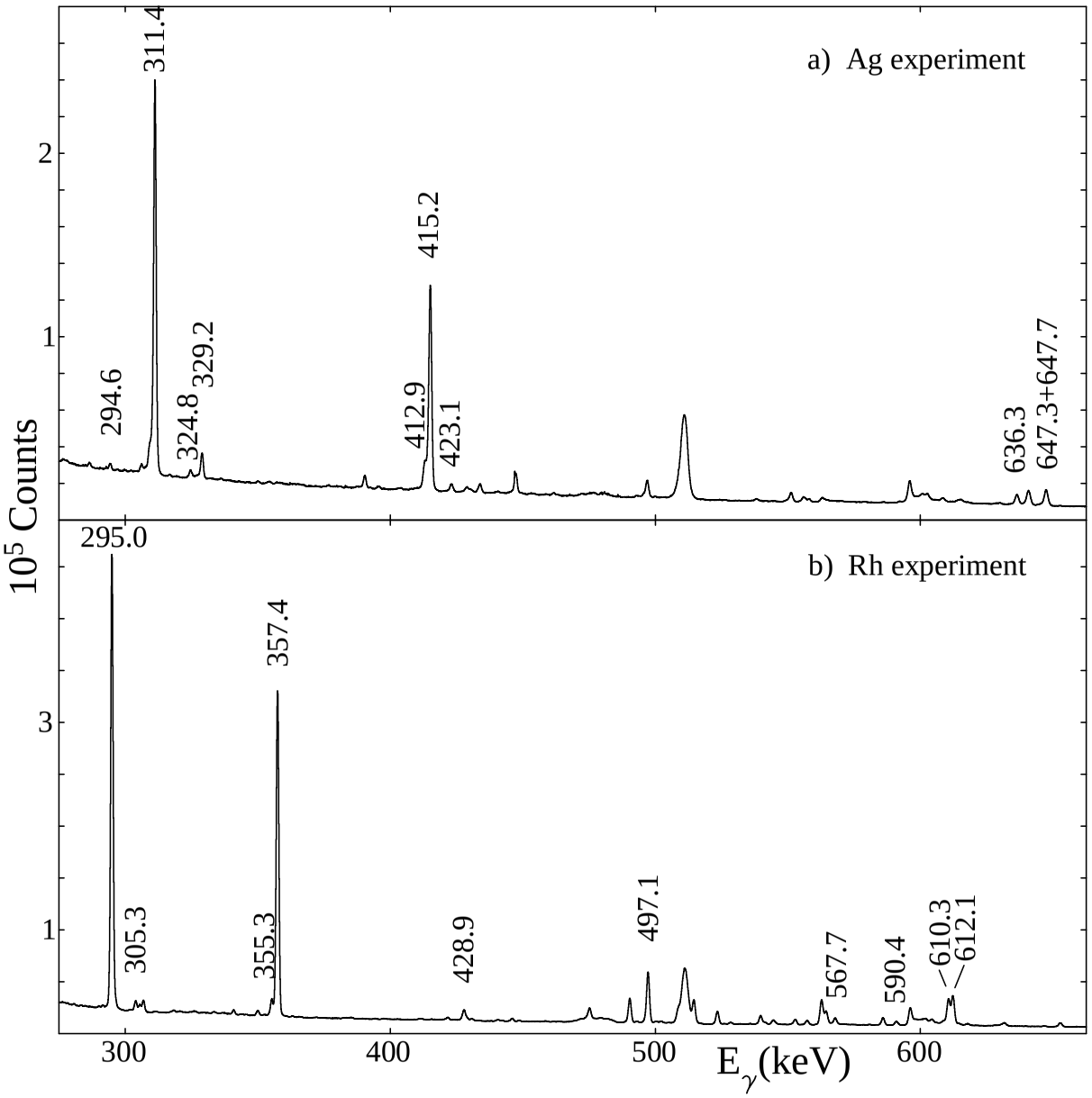

Figure 3 28Jul2016

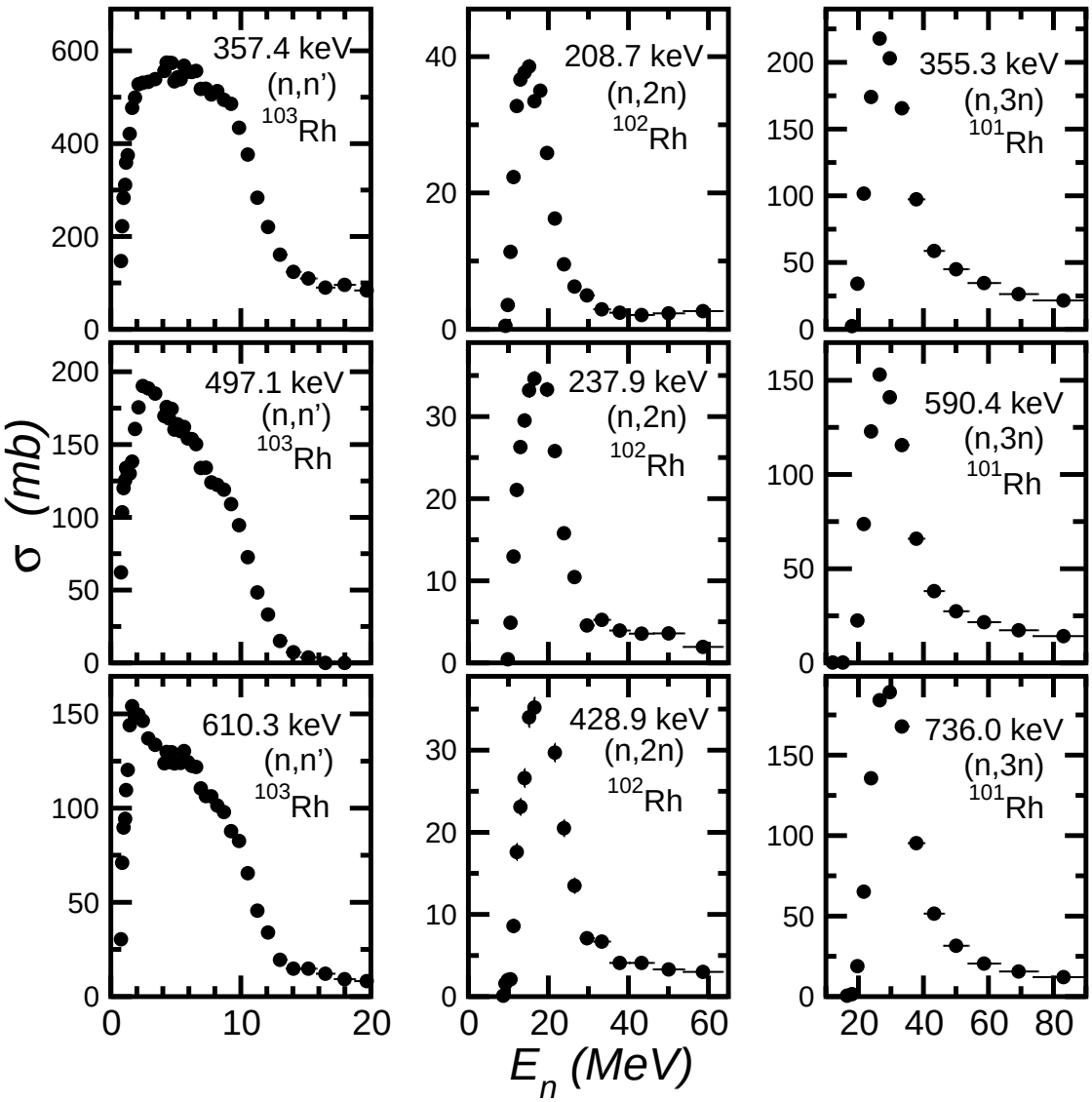

Figure 4 28Jul2016

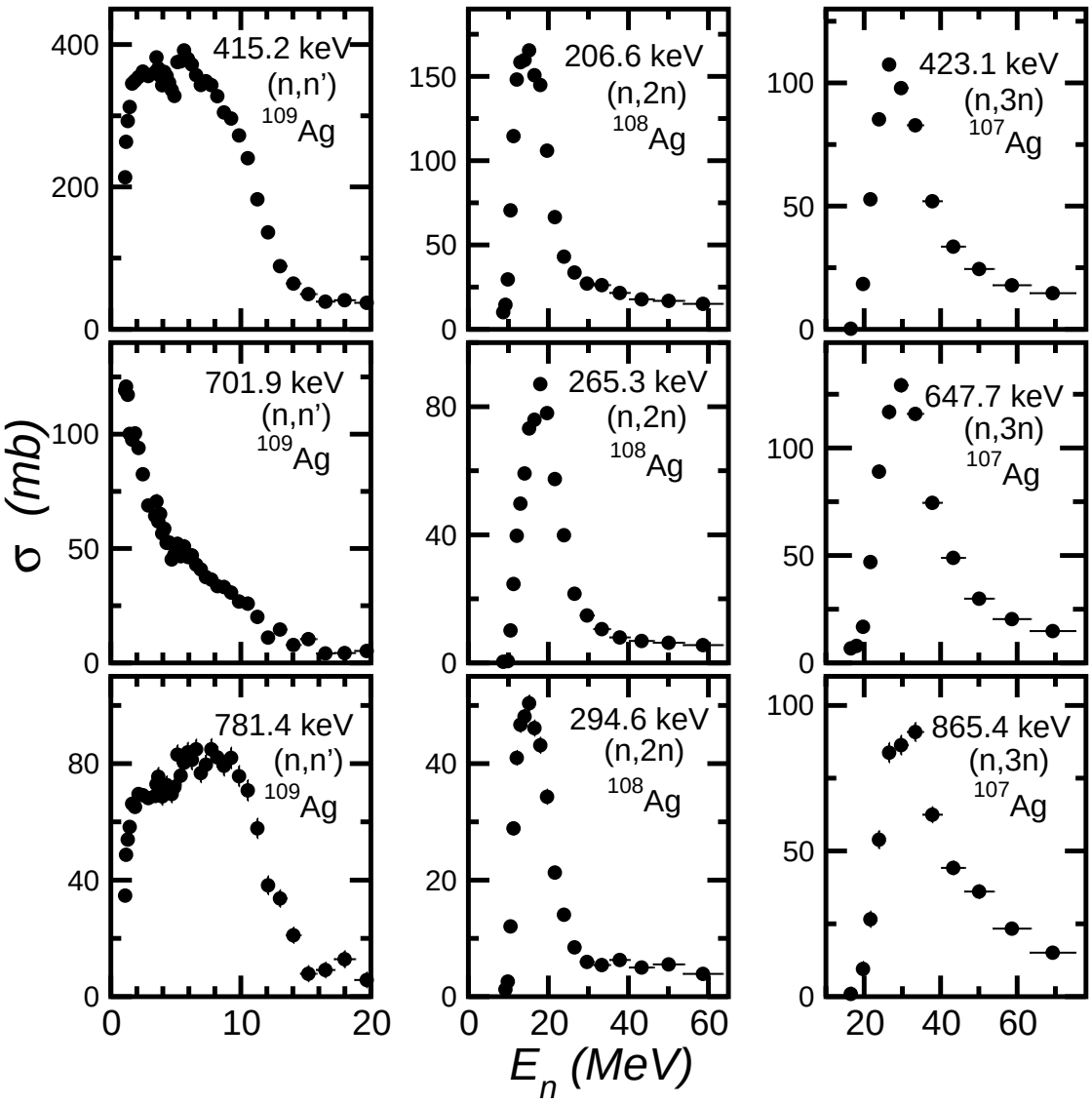

Figure 5 28Jul2016

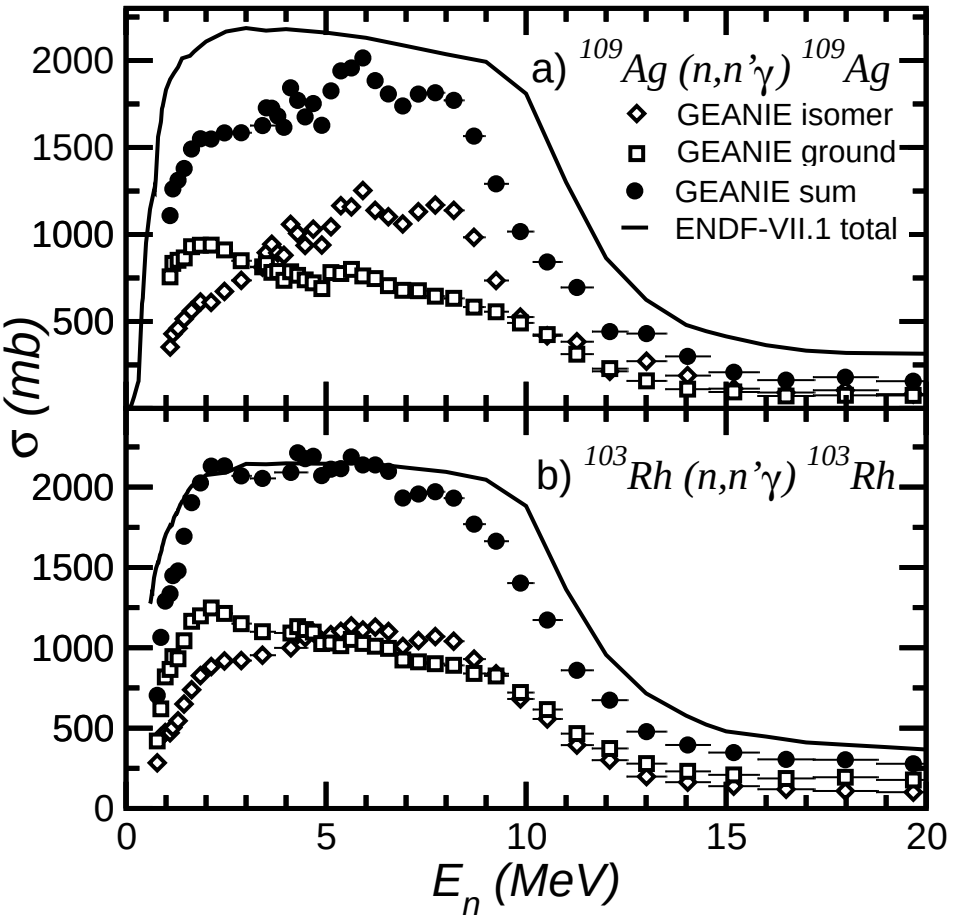

Figure 6 28Jul2016

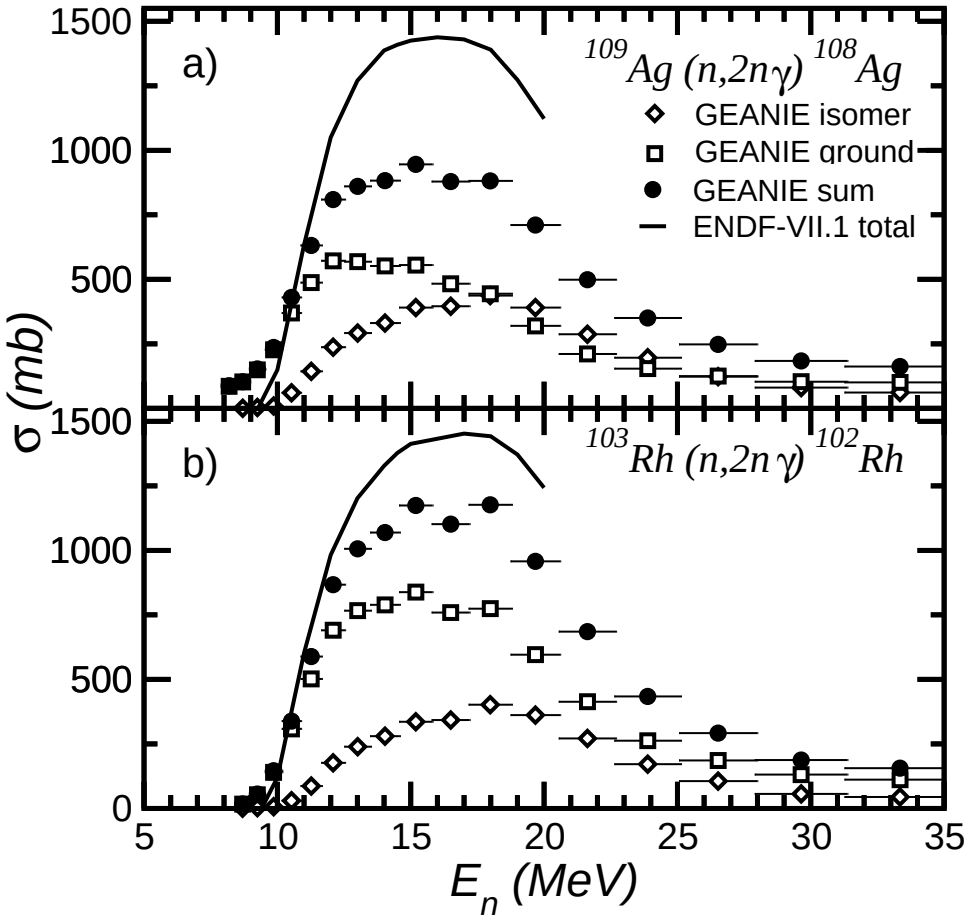

Figure 7 28Jul2016

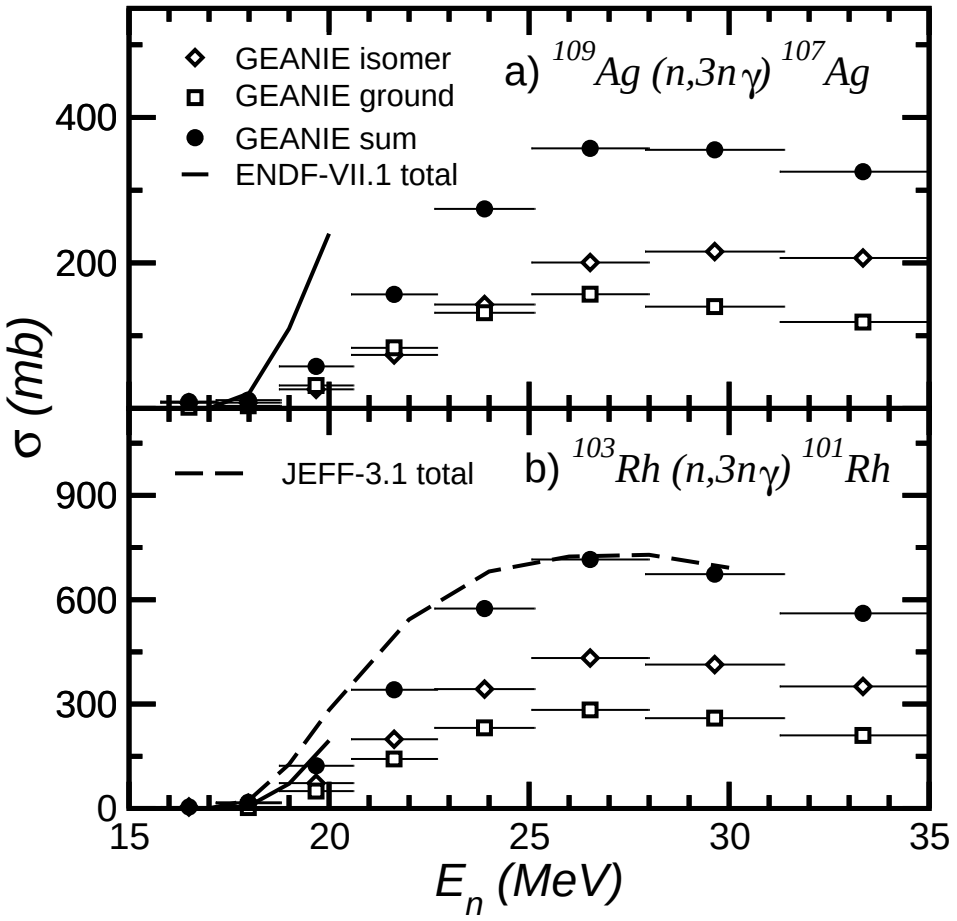

Figure 8 28Jul2016

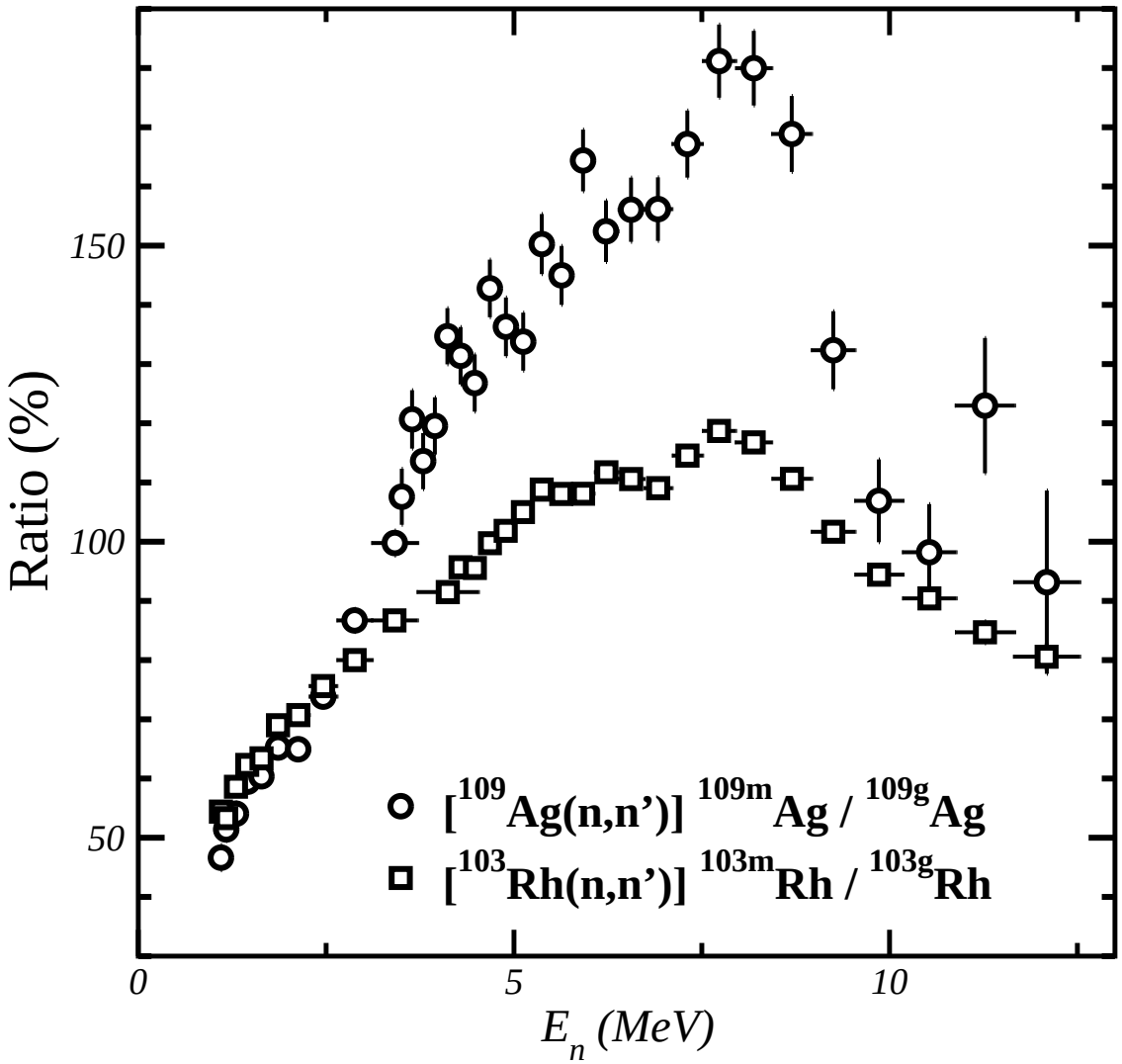

Figure 9 28Jul2016

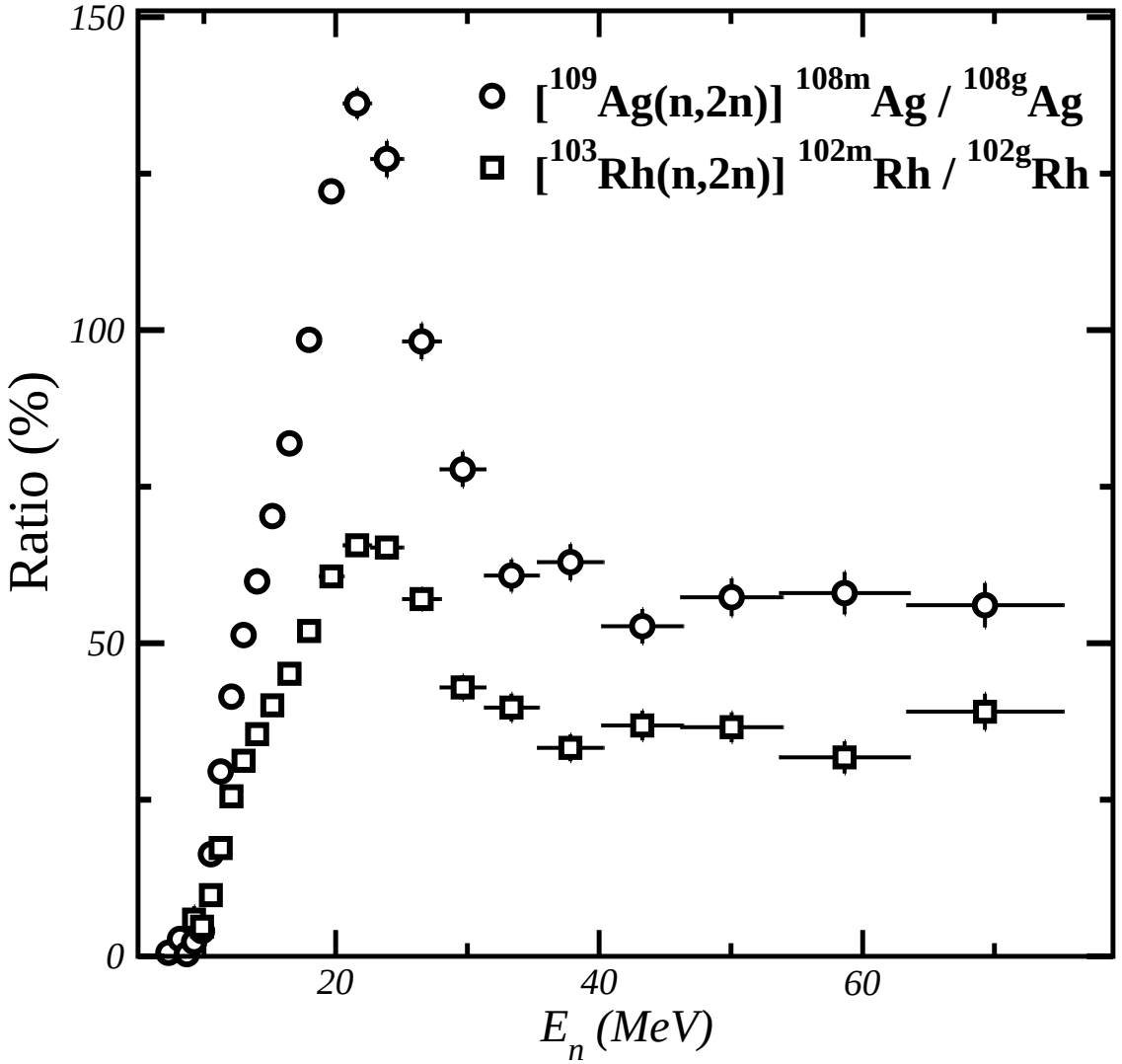

Figure 10 28Jul2016

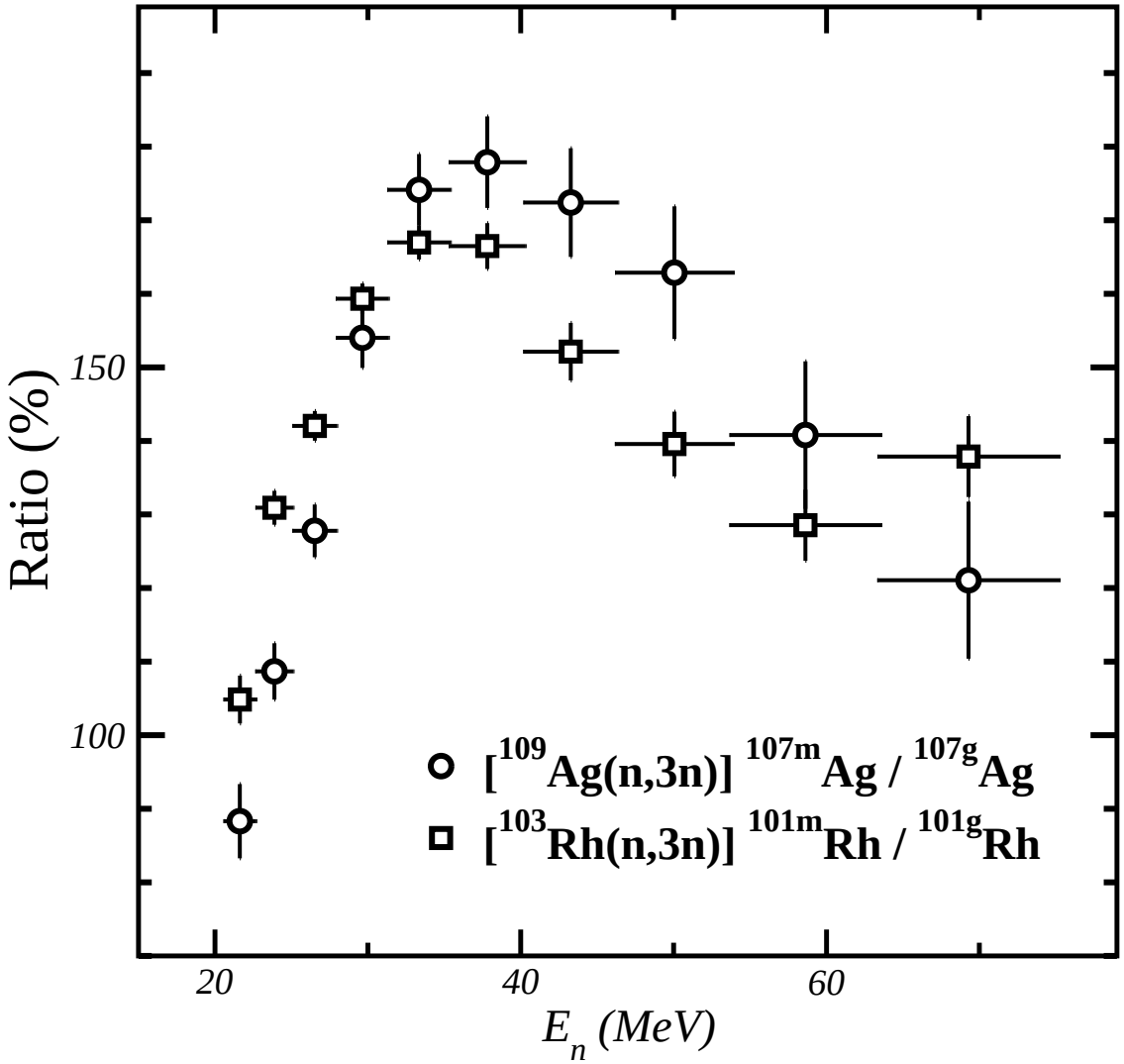

Figure 11 28Jul2016

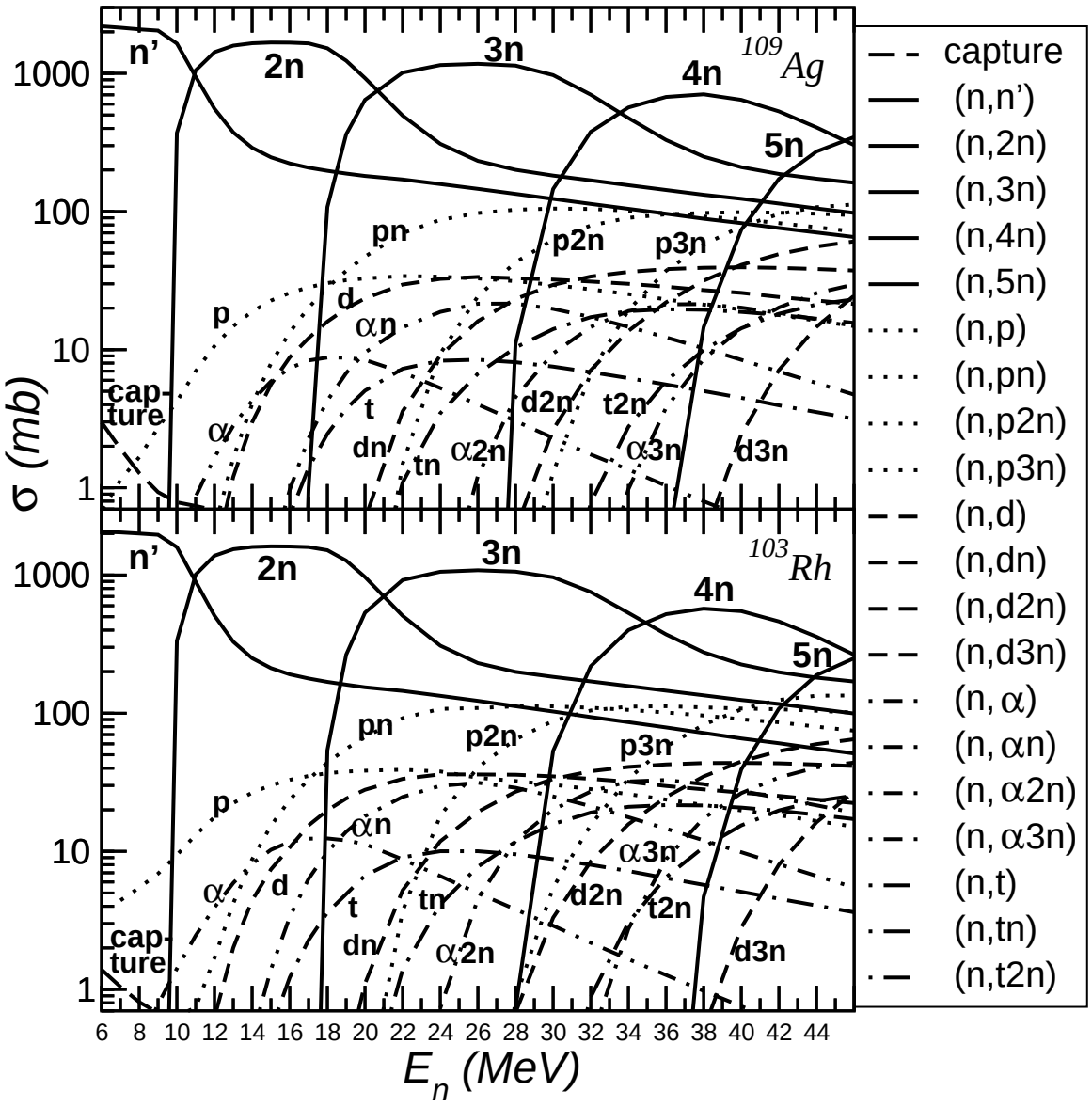

Figure 12 28Jul2016

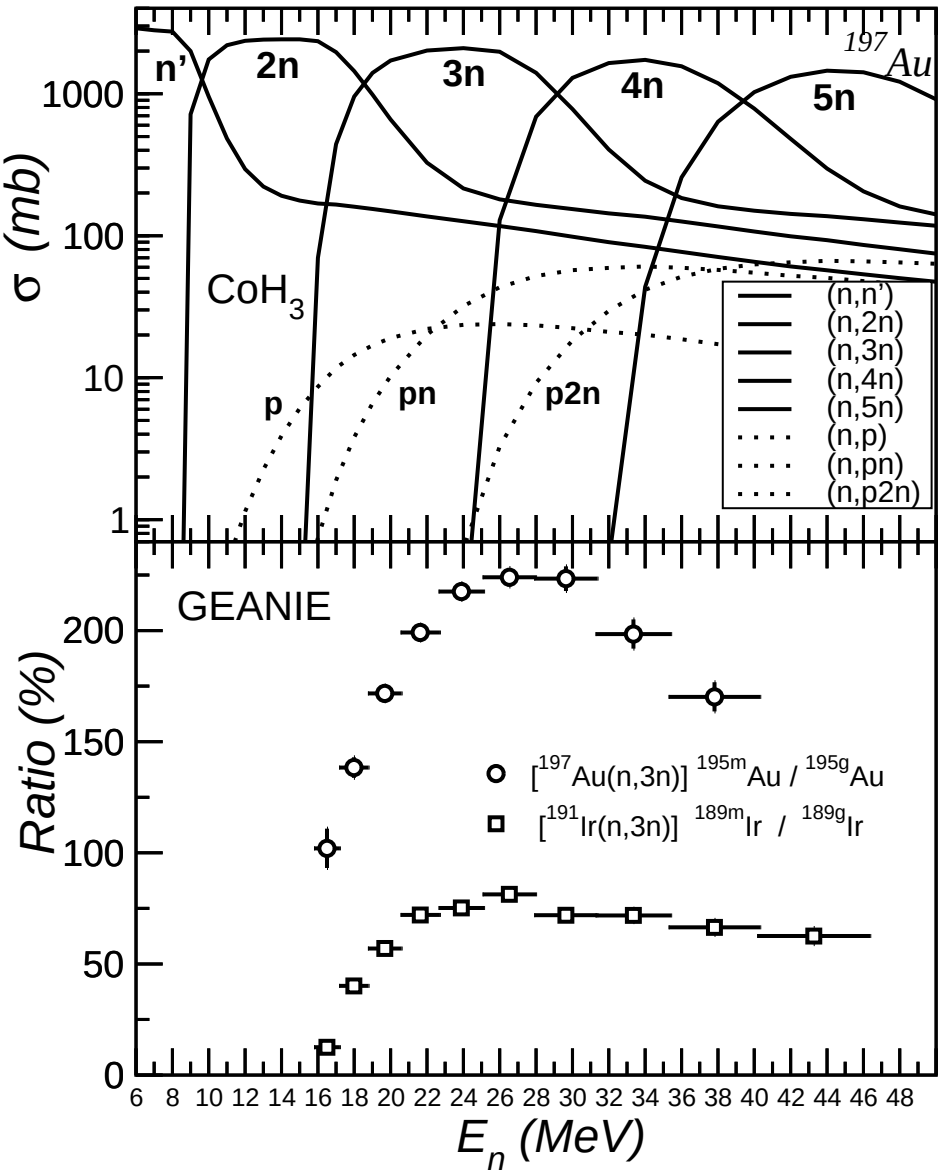

α
α
α

Figure 13 28Jul2016

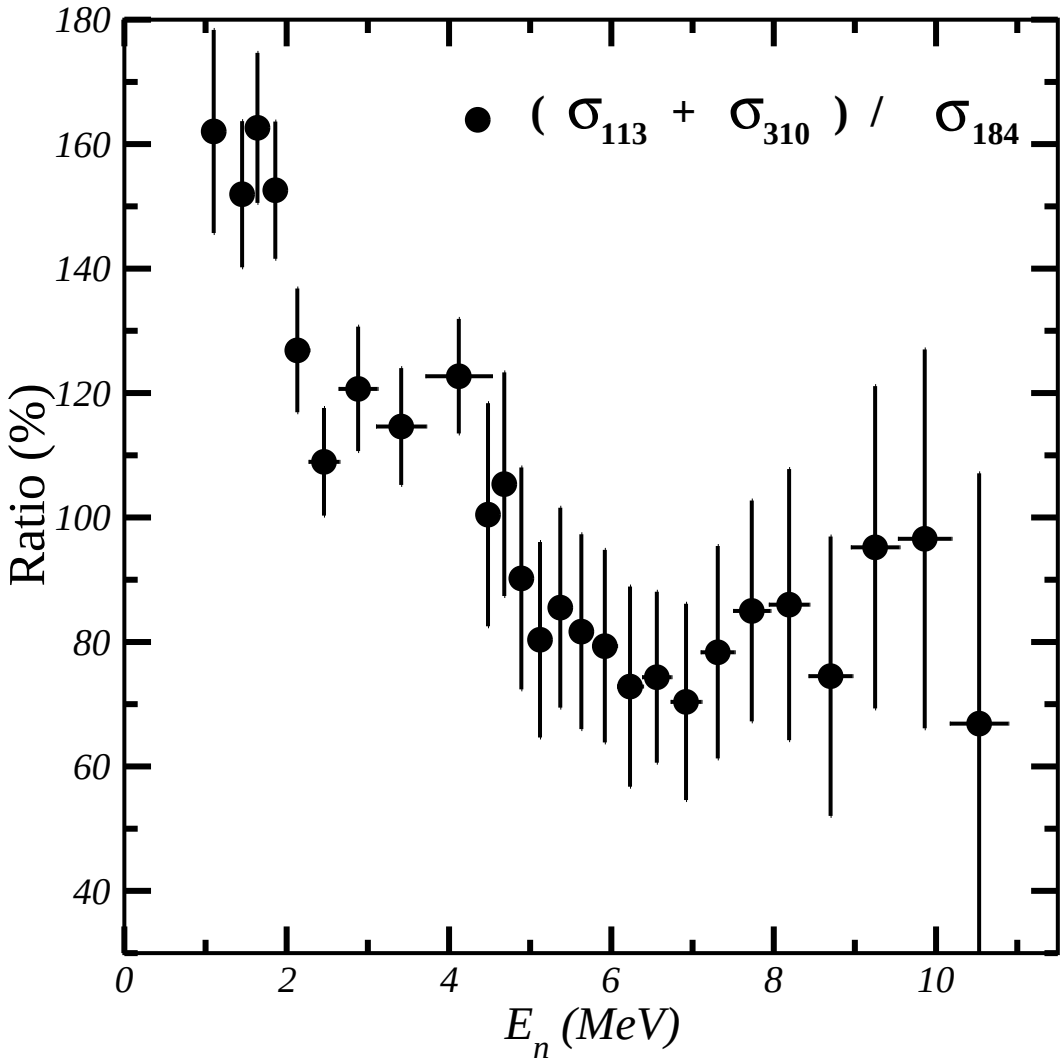

Figure 14 28Jul2016